ACS APPLIED MATERIALS & INTERFACES

Research Article

Cite This: ACS Appl. Mater. Interfaces 2019, 11, 35713−35719

www.acsami.org

Self-Optimized Catalysts: Hot-Electron Driven Photosynthesis of Catalytic Photocathodes

Evgenia Kontoleta,[§] Sven H. C. Askes,[§] and Erik C. Garnett*

Center for Nanophotonics, AMOLF, Science Park 104, 1098 XG Amsterdam, Netherlands

Supporting Information

ABSTRACT: Photogenerated hot electrons from plasmonic nanostructures are very promising for photocatalysis, mostly due to their potential for enhanced chemical selectivity. Here, we present a self-optimized fabrication method of plasmonic photocathodes using hot-electron chemistry, for enhanced photocatalytic efficiencies. Plasmonic Au/TiO_2 nanoislands are excited at their surface plasmon resonance to generate hot electrons in an aqueous bath containing a platinum (cocatalyst) precursor. Hot electrons drive the deposition of Pt cocatalyst nanoparticles, without any nanoparticle functionalization and negligible applied bias, close to the hotspots of the plasmonic nanoislands. The presence of TiO_2 is crucial for achieving higher chemical reaction rates. The Au/TiO_2/Pt photocathodes synthesized using hot-electron chemistry show a photocatalytic activity of up to 2 times higher than that of a control made with random electrodeposited Pt nanoparticles. This light-driven positioning of the cocatalyst close to the same positions where hot electrons are most efficiently generated and transferred represents a novel and simple method for synthesizing complex, self-optimized photocatalytic nanostructures with improved efficiency and selectivity.

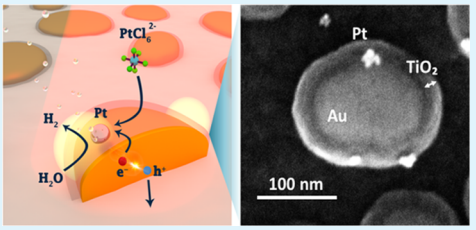

KEYWORDS: *hot-electron chemistry, plasmonic nanoparticles, photoelectrochemistry, photocatalysis, Au/TiO_2, Pt photodeposition*

INTRODUCTION

Plasmonic nanoparticles can offer alternative pathways for driving chemical reactions compared to common semiconductors. The light-controlled selectivity over chemical products on plasmonic nanoparticles makes them interesting for photocatalysis.[1−4] The different reactivity from standard thermal catalysis is thought to arise from highly energetic, "hot" electron−hole pairs formed upon plasmonic excitation and decay.[5−7] Excitation of the plasmonic nanoparticle at the resonant wavelength results in the collective coherent oscillation of conduction band electrons with a concomitant enhancement of the electric field at specific hotspots. At these hotspots, the plasmon excitation can decay via Landau damping and thereby excites a single electron to create a highly-energetic electron−hole pair, which is initially out of thermal equilibrium with the surroundings, that is, "hot".[8−10] Hot carriers from plasmonic nanoparticles have so far been used for the reduction of chemisorbed *p*-nitrothiophenol[9] or aryl diazonium salts,[11] oxidation of citrate,[12] hydrogen production,[13−16] and conversion of CO_2 to formic acid.[17]

Plasmon-driven photoelectrochemical reactions seem very promising, but the recorded efficiencies are still too low for practical use. This low efficiency is mostly due to the short hot-carrier lifetime (<3 ps for Au or Ag nanoparticles).[18−20] Higher efficiencies have been reached by bringing the metal nanostructures in contact with an appropriately chosen semiconducting layer, allowing for rapid hot-electron extraction and reduced recombination via a Schottky barrier.[8,16,19,21−25] Similarly, hot holes can be extracted with a hole-transfer layer such as nickel oxide,[15] leaving the electrons on the structure. However, hot-carrier extraction alone is often not sufficient; cocatalytic nanoparticles are necessary to achieve high efficiencies in almost all photoelectrochemical processes. Ideally, this cocatalyst has the lowest possible loading, both to reduce the amount of costly precious metals such as platinum and rhodium as well as minimize reflection and parasitic absorption of incident light. Furthermore, it should be optimum to localize the cocatalyst only near the plasmonic hotspots where hot electrons are generated most efficiently and catalysis is driven most favorably.[26−29] Nevertheless, there are few practical, low-cost, and efficient techniques to position a cocatalyst with such nanoscale precision. For instance, Mubeen et al.[16] demonstrated fully autonomous plasmonic water splitting with a Au nanorod device with two individually deposited cocatalysts. However, the fabrication techniques dictated the localization of both cocatalysts, which do not necessarily imply an optimal spatial configuration, that is, the hotspots and cocatalyst sites are potentially mismatched.

Here, we propose a self-optimized fabrication strategy where hot electrons are used both for the localized deposition of cocatalyst nanoparticles and the subsequent photocatalysis (Figure 1). Our approach removes the need for lithographic patterning of either the plasmonic nanoparticles or cocatalyst while simultaneously allowing for the ideal spatial distribution at any given loading. We used random Au plasmonic nanoislands on ITO coated with TiO_2 as the plasmonically active substrate.

Received: June 21, 2019
Accepted: September 2, 2019
Published: September 2, 2019

DOI: 10.1021/acsami.9b10913
ACS Appl. Mater. Interfaces 2019, 11, 35713−35719

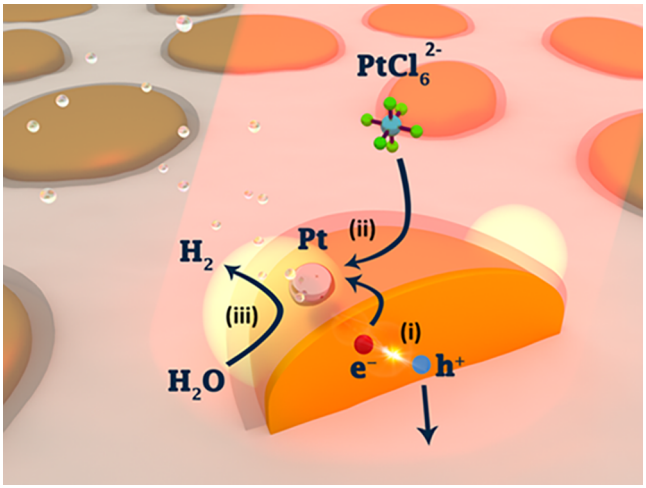

Figure 1. Schematic illustration of the self-optimized catalysts. (i) Hot electrons and hot holes are created in Au/TiO_2 nanoislands after excitation at 638 nm. (ii) Hot electrons reduce hexachloroplatinate at the plasmonic hotspots (light yellow areas) to form platinum nanoparticles (cocatalyst). (iii) Hot electrons reach the newly formed platinum nanoparticles and accelerate hydrogen production at the same excitation wavelength.

Both the deposition of Pt cocatalyst nanoparticles from solution and the subsequent photocatalysis were conducted under 638 nm illumination (within the plasmonic absorption peak). By comparing the photocatalytic performance of our self-optimized photodeposition method to that from random electrodeposition (with identical loading and dark current characteristics), we see up to a factor of 2 increase in the efficiency of photocatalysis.

EXPERIMENTAL SECTION

General Procedures. Chemicals were purchased from major chemical suppliers and used as received. Sample characterization was done with scanning electron microscopy (FEI Verios 460, acceleration beam voltage 5 kV, and beam current 100 pA), X-ray diffraction (Bruker D2 Phaser, Cu Kα radiation, and wavelength = 1.5418 Å), and atomic force microscopy (Veeco Dimension 3100 AFM). X-ray photoemission spectroscopy (XPS) was performed in a home-built ultrahigh vacuum chamber, operating at a base pressure of below 5×10^{-9} mbar. A XM1200 monochromatic X-ray source (Al α-K line, Scienta Omicron) was used for X-ray excitation of the sample under a 45° angle. Photoemitted electrons were collected using a HIPP-3 analyzer (Scienta Omicron). Spectra were charge corrected using the binding energy of 1s carbon (284.8 eV). A UV/Vis/NIR spectrophotometer (PerkinElmer, L750) was used for acquiring the absorbance spectra.

Preparation of Au Nanoislands. Plasmonic Au nanoislands were prepared on ITO-covered glass slides (Figure S1) following a literature procedure.[15] 15 × 15 mm indium tin oxide (ITO) substrates (150 nm on glass) were cleaned with detergent, rinsed with demineralized water, acetone, and isopropanol, and dried in a stream of N_2. The substrates were placed in a sputter coater (Leica EM ACE600) where 8 nm of Au was sputtered with a rate of ~0.35 nm/s and measured with a quartz crystal thickness monitor during sputtering. After deposition of the thin Au layer, the samples were placed in a tube oven, which was brought to 300 °C with a rate of 9.2 °C/min, kept at constant temperature for 1 h, and subsequently allowed to cool down to room temperature.

Atomic Layer Deposition of TiO_2 on Au Nanoislands. Atomic-layer deposition (ALD) of TiO_2 on Au nanoislands was conducted in a custom thermal ALD system developed in-house at 100 °C. The base pressure of the system was 0.03−0.07 mbar, and during deposition, the pressure was kept at 1.1 mbar with an influx of N_2. Each cycle of TiO_2 deposition consisted of injecting a 10 ms pulse of $TiCl_4$ vapor, waiting for 18 s, injecting a 10 ms pulse of H_2O vapor, and then waiting for another 18 s. The deposition rate was 0.4 Å per cycle. The TiO_2 thickness on Au nanoislands was estimated by depositing TiO_2 in parallel to a Si substrate and measuring the layer thickness by ellipsometry using a dielectric model of TiO_2 and native SiO_2 on a Si substrate. Typically, 300 cycles of TiO_2 (18 nm) were deposited on the Au nanoislands. For the purpose of electrical connection (see below), a 2 mm strip of the substrates was masked with Kapton tape during ALD.

Photoelectrodeposition of Pt on Au/TiO_2 Nanoislands. Photoelectrodeposition of platinum on Au/TiO_2 nanoisland substrates was conducted in a three-electrode photoelectrochemical cell (PEC) connected to a potentiostat (Biologic, SP-200) (Figure S2). The Au/TiO_2 substrate (working electrode) was electrically connected to the potentiostat with a conductive aluminum tape (Advance Tapes AT521) on the top 2 mm of the substrate. A rubber ring (Ø 8 mm) was placed centrally on the Au/TiO_2 working electrode, and this assembly was clamped tightly on a 6 mm hole on the outside of the electrochemical cell. Only the central 6 mm was thus in contact with the electrolyte. A leakless miniature Ag/AgCl electrode (Mengel Engineering ED-ET072) was used as a reference electrode, and a Pt wire was used as a counter electrode. The electrolyte was prepared with 100 mM Na_2SO_4 and 4 mM H_2PtCl_6 in MilliQ water (18.2 MΩ·cm) and adjusted to pH 3.0−3.4 with aliquots of NaOH (2 M). The electrolyte was prepared at least 48 h in advance to allow hydrolysis of H_2PtCl_6, which has been found important for the deposition of Pt on TiO_2.[30] The PEC was filled with an 8 mL electrolyte, and the sample was illuminated from the back without interacting first with the electrolyte with a laser beam (0.5 W/cm^2). Meanwhile, the potential of the working electrode was kept constant (chronoamperometry mode), typically at +0.25 V versus Ag/AgCl. After photoelectrodeposition, samples were rinsed with H_2O and dried with N_2.

Wavelength Dependence Measurements. Wavelength dependence measurements on Au/TiO_2 photocathodes were conducted in the presence of hexachloroplatinate under the same conditions as the photoelectrodeposition of Pt using now a different light source (supercontinuum laser, Fianium WL-SC-390-3), which was made monochromatic using an acousto-optical tunable filter (AOTF-Crystal Technologies). The signal was readout from the potentiostat (Biologic, SP-200) after lock-in amplification (Stanford Research Systems SR830), while the transmission of the AOTF was digitally modulated at 70 Hz. The potential of the working electrode was kept constant (chronoamperometry mode) at +0.25 V versus Ag/AgCl. The current measurement was started in the dark (beam was blocked manually), and every 20 s, it was alternated between a different excitation wavelength in the dark.

Electrodeposition of Pt Nanoparticles. Random deposition of platinum nanoparticles was performed on the Au/TiO_2 photocathodes in the presence of hexachloroplatinate (H_2PtCl_6, pH 3), using a pulsed electrodeposition method introduced by Liu et al.[31] Specifically, we used differential pulsed amperometry to control the sequence and the duration of the pulses sent to the sample. In the absence of light, first, a −0.6 V versus RHE potential was applied to the sample for 5 s. In sequence, the potential was changed to 0.6 V versus RHE and kept at this value for 25 s. This total period of 30 s is considered one cycle, and the amount of deposited Pt was controlled by the number of cycles.

Photoconditioning. During this step, −0.25 V versus RHE was applied to the $Pt/Au/TiO_2$ samples in the three-electrode photoelectrochemical cell in the presence of a deoxygenated (purged for 1 h with N_2) phosphate buffer (pH 7, 0.1 M). The duration of the photoconditioning step was 45 s; in the first 20 s, the sample was kept in the dark and followed by 25 s of illumination with a 638 nm beam (0.5 W/cm^2).

Photocatalysis Measurements on Au/TiO_2/Pt Photocathodes. Photocatalysis measurements of the Au/TiO_2/Pt photocathodes were conducted in the same three-electrode photoelectrochemical cell as the photoelectrodeposition of Pt nanoparticles but with a different electrolyte (phosphate buffer, pH 7, purged with nitrogen for 1 h). The current flow from the samples was measured as a function of the potential with a scan rate of 20 mV/s, under 638 nm (0.5 W/cm^2)-chopped illumination, with a chopping frequency of 25 Hz.

DOI: 10.1021/acsami.9b10913
ACS Appl. Mater. Interfaces 2019, 11, 35713−35719

FDTD Simulations of Au/TiO_2 Nanoislands. Finite difference time domain (FDTD) simulations were performed using the 3D Maxwell solver software package Lumerical. An AFM height map of Au/TiO_2 nanoislands (2 × 2 μm) was imported as a surface, which functioned as the TiO_2 layer. Optical constants retrieved by ellipsometry (Figure S3) were used for this layer. The bare Au nanoislands layer was retrieved from the same AFM height map by importing it in the 3D simulation program blender and using the displacement modifier algorithm to mimic the subtraction of the 18 nm conformal TiO_2 layer. The resulting Au nanoisland height map was exported, interpolated to uniform $x-y$ spacing using Origin software, and imported in Lumerical as a surface to function as the Au layer. Finally, an ITO substrate was added to complete the sample geometry. The background index was water (n = 1.33). The simulation space additionally consisted of a 2.3 × 2.3 × 0.5 μm (l × w × h) FDTD box with perfectly matched layer boundary conditions and a 4 × 4 nm mesh size, a 2.1 × 2.1 × 0.4 μm plane wave source at 638 nm, and a 1.8 × 1.8 × 0.2 μm advanced power absorption monitor. Here, the power absorption is proportional to the electric field intensity and imaginary part of the permittivity and is given in the fraction of absorbed power per cubic meter (P_{abs}/m^3).

Inductively Coupled Plasma Mass Spectrometry Measurements. The preparation of the samples for the inductively coupled plasma mass spectrometry (ICP-MS) measurements took place via the transfer of the glass/ITO/Au/TiO_2/Pt samples in the liquid phase. Each sample was immersed in 1 mL of an aqua regia solution, HNO_3 (≥65%, puriss. p.a.):HCl (37%) (1:3), for 5.5 h at 60 °C until the glass substrate was completely transparent. The aqua regia solution was then left to cool down overnight. The transfer of the solution was being done carefully to a centrifuge tube where it was further diluted with MilliQ water (18.2 MΩ·cm) in a total volume of 10 mL.

RESULTS AND DISCUSSION

Plasmonic Au nanoislands were prepared on ITO-covered glass slides with the aim of using them as absorbing platforms for the selective hot-electron driven deposition of the cocatalytic nanoparticles. It has already been shown that this type of sample is photocatalytic and can also support hotspots.[15,32] Briefly, an 8 nm gold film was sputtered coated on ITO substrates and subsequently annealed at 300 °C for 1 h to spontaneously form Au nanoislands (Figure 2a). The nanoislands were coated with a thin TiO_2 layer with atomic layer deposition (ALD), which acts as a hot-electron filter prohibiting recombination of the photogenerated charges in the metal by providing a high density of electron-accepting states.[33] X-ray diffraction (XRD) showed that the TiO_2 layer had crystallized in the anatase phase (Figure S4) after annealing, which has been shown to be favorable for accepting hot electrons compared to rutile or amorphous TiO_2.[34] SEM images (Figure 2a) and AFM maps (Figure 2b) showed final structures (Au/TiO_2) with a mean largest diameter of 151 ± 56 nm and a mean height of 44 ± 8 nm (Figure S5). Overlays of secondary electron and backscattered electron SEM images (Figure 2c and Figure S6) revealed the presence of a 18 ± 2 nm TiO_2 layer around the gold nanoislands, and the thickness of which was further confirmed by size distribution measurements before and after the ALD step (Figure 2d and Figure S7) and ellipsometry data (Figure S3). The chosen TiO_2 thickness arose from preliminary results for optimization of the photocurrent of our system (see below).

Absorption spectra showed a strong plasmonic peak of the Au/TiO_2 structures centered between 640 and 700 nm, depending on small sample thickness differences (Figure 2e), which is an ideal wavelength range for the generation of hot electrons, as plasmonic excitations below 600 nm are strongly dampened by interband transitions in bulk Au.[35,36] The size distribution of the nanostructures could strongly affect the

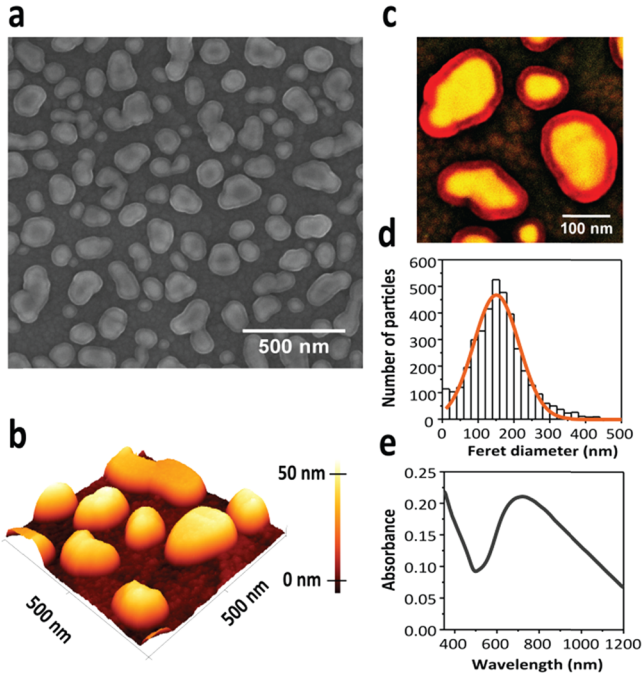

Figure 2. Characterization of Au/TiO_2 nanoislands on ITO/glass substrate. (a) SEM image, (b) AFM map, (c) overlay of backscattered (yellow) and secondary electron (red) images where the strong contrast between TiO_2 and Au nanoislands originates from the lack of electron backscatter by the lighter elements of the TiO_2 shell, (d) size distribution of Au/TiO_2 nanoislands after SEM imaging analysis with a fitting Gaussian curve (orange solid line), and (e) absorbance spectrum.

surface plasmon resonance of the final samples and could be easily tuned by altering the thickness of the sputter-coated Au film. The size distribution chosen here gave a resonance far from the interband transition wavelength region but still in a high electron energy range. A redshift and a broadening of the absorption peak of the Au nanoislands were observed (Figure S8) after the addition of TiO_2, which can be attributed to the higher embedding refractive index and possibly also to increased interparticle coupling.[32,37] The TiO_2 layer has negligible optical absorption at 638 nm with an onset of band gap absorption in the ultraviolet, as expected (Figure S3). When deposited on ITO, there is some parasitic absorption, but this is far below (~9 times) than that of the plasmonic nanoislands (Figure S8) and does not contribute significantly to photocurrent (Figure S9). The Au/TiO_2 nanoislands were easily prepared on a bulk scale and were suitable for studying hot-electron photoreactions with red light.

The ability of Au/TiO_2 nanoislands to generate hot e^-, which can drive a chemical reaction for the synthesis of cocatalytic nanoparticles, was investigated. The nanoislands were excited by a 638 nm laser beam (0.5 W/cm^2) in a three-electrode photoelectrochemical cell under a potentiostatic control using a Ag/AgCl reference electrode. The current flow from the sample (working electrode) to a platinum wire (counter electrode) was recorded in the presence of an aqueous platinum precursor (0.04 mM H_2PtCl_6 in 0.1 M Na_2SO_4, pH 3, and deoxygenated). At open-circuit voltage conditions (OCV = 470−580 mV vs RHE), a very little photocurrent was observed, but sweeping the potential to more negative values increased the Pt photodeposition rate (Figure S9c). Figure 3a shows a typical current density versus time curve of the Au/TiO_2 nanoislands both under 638 nm light illumination (laser on) and in the dark

DOI: 10.1021/acsami.9b10913
ACS Appl. Mater. Interfaces 2019, 11, 35713−35719

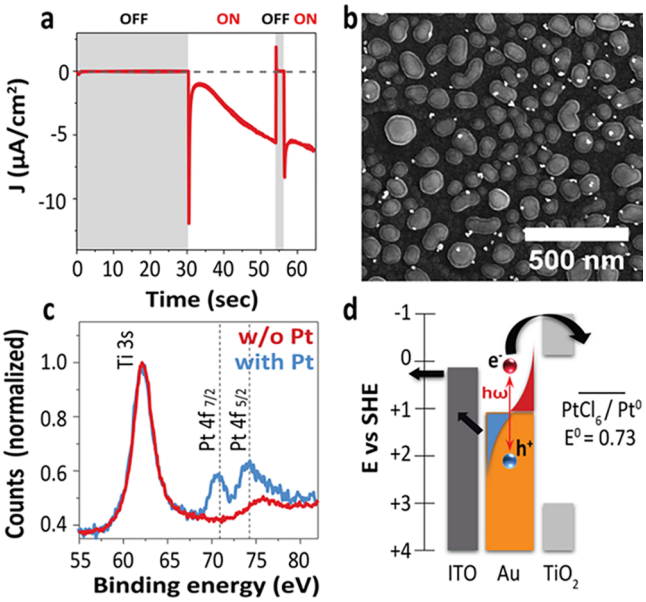

Figure 3. (a) Current density vs time plot of Au/TiO_2 nanoislands in presence of hexachloroplatinate (pH 3, 0.04 mM in 0.1 M Na_2SO_4 aqueous solution, and 450 mV vs RHE). (b) SEM image of Pt nanoparticles on Au/TiO_2 nanoislands after illumination of the latter at 638 nm (0.5 W/cm^2) in hexachloroplatinate and recording of 125 μC/cm^2 of electrical charge from the sample. (c) X-ray photoemission spectrum of the samples before (light blue line) and after photoelectrodeposition of Pt nanoparticles (red line). Dashed lines indicate literature values for metallic Pt $4f_{7/2}$ and $4f_{5/2}$ binding energies.[44] (d) Simplified band diagram of Au/TiO_2 nanoislands on ITO and flow of hot electrons and holes during the photoelectrodeposition process.

(laser off) at 450 mV versus RHE. While the dark current was negligible throughout the whole measurement, the photocurrent gradually increased as a function of time (t = 30−55 and 55−65 s, Figure 3a). Furthermore, almost no photocurrent (~16 nA/cm^2, 40−1000 times lower than Au/TiO_2 samples) was recorded from bare TiO_2 (Figure S9), indicating that the photoactivity comes from plasmonic absorption in the Au and hot-electron photoreduction. In our approach, current measurements are retrieved from the whole photoelectrode, a bulk method that has already been used as evidence for hot-electron flow.[15,16,38] Single-nanoparticle photocurrent measurements have also confirmed that the presence of photocurrent at the surface plasmon resonance of the nanostructure is related to the flow of hot carriers.[39]

SEM images showed that after an electrical charge of 125 μC/cm^2 was passed to the sample, new nanoparticles appeared on the Au/TiO_2 samples (bright clusters, Figure 3b). The newly formed nanoparticles corresponded to a mixture of Pt(II)/Pt(IV) salts/oxides according to XPS (Figure S10) and EDX measurements (Figure S11), so they were further reduced by a "photoconditioning" step and using again hot-electron chemistry. During this step, the platinum-containing electrolyte was exchanged with an aqueous phosphate buffer to avoid further deposition of Pt species, and the sample was irradiated for 25 s at 638 nm (0.5 W/cm^2) at an applied potential of −250 mV versus RHE (Figure S12). After the photoconditioning procedure, the observed platinum $4f_{7/2}$ and $4f_{5/2}$ binding energy peaks matched a metallic Pt reference (Figure 3c), indicating that the reduced particles consisted mainly of metallic platinum, favorable for catalyzing many chemical reactions.[40] The fact that the initial photoreaction did not produce any metallic Pt may be ascribed to Pt^{4+} kinetically outcompeting Pt^{2+} species for hot electrons. However, photoconditioning at the same potential as the initial photodeposition step (450 mV) did not result in Pt^0 nanoparticles. This indicates that it is the extra potential is crucial for the full reduction of Pt species. Apparently, hot electrons that have been injected in the TiO_2 conduction band do not possess sufficient reducing power to fully reduce hexachloroplatinate to metallic platinum. These results mirror those from Xi et al.[30] who have shown that the electrochemical reduction of hexachloroplatinate leads to mixed valence materials. More reducing potentials (than −250 mV vs RHE) were avoided during the photoconditioning step, because then, the distinction between hot electron mechanism and bare electrochemical reduction of Pt species would be difficult. As a result, the photocurrent measured in the Au/TiO_2 nanoislands could eventually be correlated with the deposition of Pt nanoparticles.

We thus examined the correlation of the photocurrent generation (i.e., the hot-electron production) with the absorptance of the Au plasmonic nanoislands. Au nanoislands coated with TiO_2 were excited at different wavelengths (440−760 nm, with 20 nm step) with a supercontinuum laser, while the current was recorded (Figure S13) in the presence of hexachloroplatinate. The incident photon to current efficiency (IPCE) was calculated (see the Supplementary Information for more information) for every excitation wavelength and plotted together with the absorptance spectrum of the same sample as a function of the wavelength (Figure S14). The results show that there is a good correlation between the absorptance of the Au nanoislands and the IPCE values, except for in the blue region (440−500 nm). Seemingly, photogenerated electrons resulting from interband transitions (high energy electrons) barely participate in the photoreduction of hexachloroplatinate. This is reasonable since these electrons are excited from d band levels to energy levels close to or below the Fermi level of Au.[19] These electrons therefore do not have enough energy to surpass the Au/TiO_2 Schottky barrier and contribute to the generation of photocurrents. So, apparently only hot electrons with energy high enough to be injected to the conduction band of TiO_2 can reach the hexachloroplatinate molecules and reduce them to Pt species.

The plasmonic excitation of Au nanoislands clearly leads to Pt nanoparticle formation, but to further confirm that this occurs via a hot-electron mechanism, we have conducted several control experiments. The most obvious alternative explanation is a simple heating effect. The large increase in photocurrent after the addition of TiO_2 (Figure 3a and Figure S9) as well as the correlation between the absorptance and IPCE spectra (Figure S14) already point toward a hot electron rather than a thermal mechanism. Hot electrons with energy high enough to overcome the Schottky barrier are transferred into the TiO_2 layer where the barrier reduces the chances of back transfer and recombination, increasing the efficiency of Pt formation (Figure 3d). The improved yield of Pt with the addition of TiO_2 alone cannot completely rule out a thermal effect since hexachloroplatinate molecules bind much better to the TiO_2 surface than on Au, which allows for suitable electron acceptors being always present as the hot electron arrives at the TiO_2/H_2O interface.[34] However, the better surface binding cannot explain the correlation between the absorption and IPCE spectra described above. Additionally, the photocurrent showed a linear dependence on the laser intensity over a range of two orders of magnitude (Figure S15), consistent with a hot-electron

DOI: 10.1021/acsami.9b10913
ACS Appl. Mater. Interfaces 2019, 11, 35713−35719

mechanism and inconsistent with laser heating.[7,38] The temperature on the surface of the sample was measured with a FLIR thermal camera (Figure S16) during irradiation at 638 nm (0.5 W/cm^2) and reached up to 30 °C. As a follow-up control test, we conducted dark heating experiments and saw no Pt nanoparticle formation at 40 °C even after 20 min (Figure S17), showing that thermal decomposition is not playing a role in our experiments.

The observed photocurrent density increase as a function of time during the photoelectrodeposition of Pt on the Au/TiO_2 nanoislands (Figure 3a) can be explained by the presence of the first atoms of Pt formed on the surface of TiO_2 acting as electron sinks and enhancing the reaction rate.[41] The sudden current transient ("spikes" at 30 and around 55 s, Figure 3a) every time the laser is switched on could be the result of charge recombination at the electrode/electrolyte interface. As a function of time, the amplitude of the current transients seems decreased (~ 55 sec), and this could be correlated with the presence of the first Pt atoms, which reduce the charge recombination and improve the separation of the hot electrons from the hot holes.[42] The correlation between plasmonic hotspots and Pt deposition sites was unfortunately very challenging to be investigated because the hotspots were not very well defined. In addition, FDTD simulations of the three-dimensional AFM-deduced structures (without Pt deposits) showed that the hotspots on this type of nanostructures are generally spread out across large distances around the nanoparticle edges (Figures S18 and S19). In Figure 3b, some Pt nanoparticles form in areas between the Au nanoislands where no plasmonic hotspots appear according to FDTD simulations, and the enhancement of the absorbed power is mostly observed on the Au nanoislands (Figures S18 and S19). This indicates that hot electrons injected into the TiO_2 layer can diffuse and form Pt nanoparticles that somewhat removed from the plasmonic hotspots, in contrast with previous reports where TiO_2 was not used.[43] Nevertheless, even in the case that hot electrons are reaching the electrolyte and reducing hexachloroplatinate further from the actual hotspots, the positioning of the cocatalyst can be still considered as optimum for the photocathode as a whole. Hot electrons are created and then diffused until they meet a site that supports an efficient transfer to the photoelectrode surface. After further illumination of the Au/TiO_2/Pt photocathodes, the new photogenerated hot electrons will probably follow the same path as the first time to the electrolyte but now meeting the cocatalyst nanoparticles first. In that way, the whole process is not limited by the exact characteristics of the TiO_2 film but enables any imperfections "work" in its favor.

To illustrate the photocatalytic behavior of the hot-electron driven prepared photocathodes (Au/TiO_2/Pt_{photo}), we performed current density versus potential (CV) scans in the presence of an aqueous phosphate buffer (0.1 M, pH 7, and deoxygenated). The current flow of the Au/TiO_2/Pt_{photo} samples was recorded under chopped illumination at 638 nm while sweeping the electrochemical potential of the working electrode to more negative (reducing) values (Figure 4a,b, blue solid line). The CV scan shows an increase in the current density under illumination (laser on), which becomes higher toward more negative potentials. The dark current (laser off) remains negligible (~130 times lower than the photocurrent) until an applied potential of around −0.35 V versus RHE where it starts increasing rapidly. The difference between onset potential of photo and dark current can be explained by the Schottky barrier

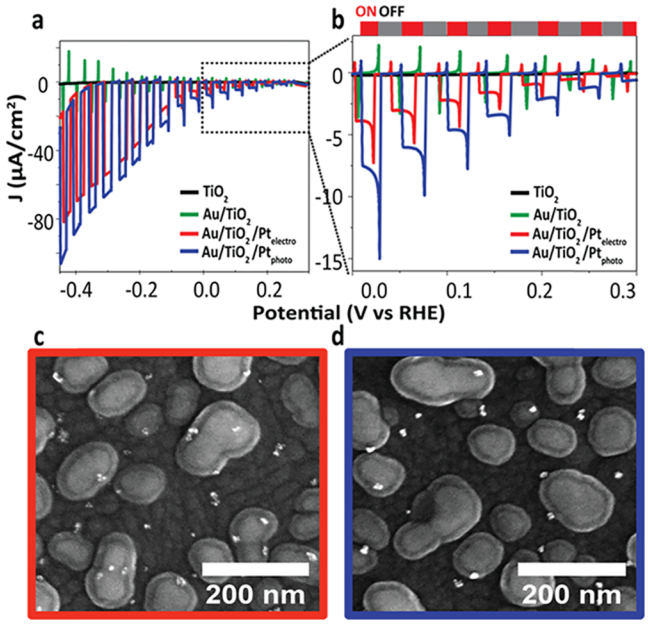

Figure 4. (a) Current density vs potential plots of TiO_2 (black solid line), Au/TiO_2 nanoislands (green solid line), Au/TiO_2 nanoislands with randomly electrodeposited Pt nanoparticles (Au/TiO2/$Pt_{electro}$, solid red line), and localized photoelectrodeposited Pt (Au/TiO_2/Pt_{photo}, solid blue line) in pH 7 phosphate buffer under chopped 638 nm illumination (0.5 W/cm^2). (b) Zoom-in of plot (a) at low applied potentials (0.0−0.3 V vs RHE). (c, d) SEM images of Au/TiO_2/$Pt_{electro}$ and Au/TiO_2/Pt_{photo} photocathodes, respectively.

between Au and TiO_2. The more negative the applied potential, the smaller the Au/TiO_2 Schottky barrier due to the shift of the Fermi level of Au toward the vacuum level and the conduction band of TiO_2.[45] In the absence of light, the Au/TiO_2 Schottky barrier does not allow electrons to flow from Au to TiO_2 and drives the chemical reaction, so almost no current is recorded until the Fermi level of Au equalizes with the conduction band of TiO_2 at −0.3 V versus RHE. Assuming a Fermi−Dirac hot-electron distribution in the Au nanoparticles under illumination,[5] more electrons will have high enough energy for transfer to the TiO_2, increasing the photocurrent. Control measurements were also conducted on bare TiO_2 as well as Au/TiO_2 to investigate performance without the cocatalyst and plasmonic light absorber, respectively. CV scans on both of these configurations (Figure 4a,b, black and green solid lines, respectively) revealed that the recorded photocurrent was ~1000 and ~30 times lower, for TiO_2 (~4 nA) and Au/TiO_2 (140 nA), respectively, than those for the Au/TiO_2/Pt_{photo} samples at 0 V versus RHE. This proves that both the plasmonic absorber and cocatalyst play key roles in the photocatalytic behavior. Considering the potential onset of the photoreduction reaction and the species available in solution, water reduction to hydrogen is the most likely photochemical reaction product.

To test the self-optimized behavior of our approach, we investigated if our method of preparing photocathodes with hot-electron injection performs better in photocatalysis than that of a common electrodeposition method of depositing the cocatalyst (see the Supporting Information for more details) under the same conditions. To warrant a valid comparison, we carefully controlled the electrodeposition conditions to achieve samples with an identical amount of platinum, with the same morphology and oxidation state, verified by ICP-MS, XPS, and SEM (Table S2, Figure S20, and Figure 4c,d). CV scans (Figure

DOI: 10.1021/acsami.9b10913
ACS Appl. Mater. Interfaces 2019, 11, 35713−35719

4a,b, blue and red solid lines) showed that when we let the plasmonic nanostructures decide where the cocatalyst will be deposited (i.e., hot-electron deposition, $Au/TiO_2/Pt_{photo}$), the photocurrent density was higher (up to 2 times) than when the cocatalyst was randomly electrodeposited ($Au/TiO_2/Pt_{electro}$), especially at small applied potentials. This suggests that the localization of the cocatalyst close to the hotspots of the plasmonic photocathodes, where the hot electrons reach the photocathode/electrolyte interface, promotes the chemical reaction. The positioning of the cocatalyst exactly on the pathway of the photogenerated hot electrons toward the electrolyte could contribute to the better utilization of the hot electrons participating in the chemical reaction. In case of a random cocatalyst distribution on the plasmonic photocathodes, the hot electrons will have to diffuse further than their original path to find the cocatalyst. During this additional diffusion, the probability of their recombination with the respective hot holes, remaining in the gold, is increased. The potential dependence of the photocurrent varied somewhat from sample to sample (Figure 4a, Figures S21 and S22), suggesting that the hot-electron energy distribution is sensitive to the exact Au nanoisland geometry and/or differences on the TiO_2 surface. Therefore, only samples, which had exactly the same amount of deposited platinum (retrieved from XPS, Figures S20, S21, and S22 and ICP-MS data, and Table S2) and the same dark current (see CV scans for photoelectrodeposited and electrodeposited samples, Figures S21 and S22) were compared. Further work trying to use this potential distribution to map out hot-electron energy distributions is ongoing.

CONCLUSIONS

In summary, we demonstrate a lithography-free method for creating plasmonic photocathodes with cocatalyst nanoparticles placed selectively at hot-electron generation sites. The plasmonic hotspots on Au/TiO_2 nanoislands were used both to localize the Pt nanoparticle cocatalyst and to do photocatalysis. The presence of TiO_2 proved to be essential for reducing recombination of hot carriers and led to higher photocurrent values. Besides providing a good hot-electron filter, the TiO_2 may also enhance binding of the Pt precursor molecules on its surface. We also showed that photocathodes with a cocatalyst deposited using hot electrons have better photocatalytic performance than those made with randomly placed electrodeposited Pt. This self-optimized photoelectrode strategy, where plasmonic nanostructures themselves determine the cocatalyst position, is a very promising route for simple fabrication of complex photocatalytic nanostructures that could lead to enhanced plasmonic solar fuel production.

ASSOCIATED CONTENT

Supporting Information

The Supporting Information is available free of charge on the ACS Publications website at DOI: 10.1021/acsami.9b10913.

Description of the ICPE calculation as well as extra experiments and characterization (ICP-MS, EDX, XRD, ellipsometry, and XPS) of the samples and FDTD simulation setup (PDF)

AUTHOR INFORMATION

Corresponding Author

*E-mail: E.Garnett@amolf.nl.

ORCID

Evgenia Kontoleta: 0000-0002-3327-1523
Sven H. C. Askes: 0000-0001-6538-3645
Erik C. Garnett: 0000-0002-9158-8326

Author Contributions

§E.K. and S.A. contributed equally.

Notes

The authors declare no competing financial interest.

ACKNOWLEDGMENTS

We thank Reinout Jaarsma (Advanced Research Center for Nanolithography: ARCNL institute) for his technical assistance with the XPS measurements, Jan Zomerdijk (AMOLF institute) for his help with the electrical measurements, and Peter Nobels (Chemical Biological Soil Laboratory, Wageningen University and Research) for the conduction of the ICP-MS measurements. We also acknowledge Dr. Andrea Baldi (Dutch Institute for Fundamental Energy Research) and Dr. Marco Valenti (AMOLF) for the useful discussions. This work is part of the research program of the Foundation for Fundamental Research on Matter (FOM), which is financially supported by the Netherlands Foundation for Scientific Research (NWO).

REFERENCES

(1) Zhang, X.; Li, X.; Zhang, D.; Su, N. Q.; Yang, W.; Everitt, H. O.; Liu, J. Product Selectivity in Plasmonic Photocatalysis for Carbon Dioxide Hydrogenation. *Nat. Commun.* **2017**, *8*, 14542.

(2) Linic, S.; Aslam, U.; Boerigter, C.; Morabito, M. Photochemical Transformations on Plasmonic Metal Nanoparticles. *Nat. Mater.* **2015**, *14*, 567−576.

(3) Marimuthu, A.; Zhang, J.; Linic, S. Tuning Selectivity in Propylene Epoxidation by Plasmon Mediated Photo-Switching of Cu Oxidation State. *Science* **2013**, *339*, 1590−1593.

(4) Quiroz, J.; Barbosa, E. C. M.; Araujo, T. P.; Fiorio, J. L.; Wang, Y. C.; Zou, Y. C.; Mou, T.; Alves, T. V.; De Oliveira, D. C.; Wang, B.; Haigh, S. J.; Rossi, L. M.; Camargo, P. H. C. Controlling Reaction Selectivity over Hybrid Plasmonic Nanocatalysts. *Nano Lett.* **2018**, *18*, 7289−7297.

(5) Boriskina, S. V.; Ghasemi, H.; Chen, G. Plasmonic Materials for Energy: From Physics to Applications. *Mater. Today* **2013**, *16*, 375−386.

(6) Wang, P.; Huang, B.; Dai, Y.; Whangbo, M.-H. Plasmonic Photocatalysts: Harvesting Visible Light with Noble Metal Nanoparticles. *Phys. Chem. Chem. Phys.* **2012**, *14*, 9813−9825.

(7) Christopher, P.; Xin, H.; Marimuthu, A.; Linic, S. Singular Characteristics and Unique Chemical Bond Activation Mechanisms of Photocatalytic Reactions on Plasmonic Nanostructures. *Nat. Mater.* **2012**, *11*, 1044−1050.

(8) Clavero, C. Plasmon-Induced Hot-Electron Generation at Nanoparticle/Metal-Oxide Interfaces for Photovoltaic and Photocatalytic Devices. *Nat. Photonics* **2014**, *8*, 95−103.

(9) Cortés, E.; Xie, W.; Cambiasso, J.; Jermyn, A. S.; Sundararaman, R.; Narang, P.; Schlücker, S.; Maier, S. A. Plasmonic Hot Electron Transport Drives Nano-Localized Chemistry. *Nat. Commun.* **2017**, *8*, 14880.

(10) Forcherio, G. T.; Baker, D. R.; Boltersdorf, J.; Leff, A. C.; McClure, J. P.; Grew, K. N.; Lundgren, C. A. Targeted Deposition of Platinum onto Gold Nanorods by Plasmonic Hot Electrons. *J. Phys. Chem. C* **2018**, *122*, 28901−28909.

(11) Nguyen, V. Q.; Ai, Y.; Martin, P.; Lacroix, J. C. Plasmon-Induced Nanolocalized Reduction of Diazonium Salts. *ACS Omega* **2017**, *2*, 1947−1955.

(12) Schlather, A. E.; Manjavacas, A.; Lauchner, A.; Marangoni, V. S.; DeSantis, C. J.; Nordlander, P.; Halas, N. J. Hot Hole Photoelectrochemistry on Au@SiO2@Au Nanoparticles. *J. Phys. Chem. Lett.* **2017**, *8*, 2060−2067.

DOI: 10.1021/acsami.9b10913
ACS Appl. Mater. Interfaces 2019, 11, 35713−35719

(13) Wang, F.; Wong, R. J.; Ho, J. H.; Jiang, Y.; Amal, R. Sensitization of Pt/TiO_2 Using Plasmonic Au Nanoparticles for Hydrogen Evolution under Visible-Light Irradiation. *ACS Appl. Mater. Interfaces* **2017**, *9*, 30575−30582.
(14) Wan, D. Y.; Zhao, Y. L.; Cai, Y.; Asmara, T. C.; Huang, Z.; Chen, J. Q.; Hong, J.; Yin, S. M.; Nelson, C. T.; Motapothula, M. R.; Yan, B. X.; Xiang, D.; Chi, X.; Zheng, H.; Chen, W.; Xu, R.; Ariando; Rusydi, A.; Minor, A. M.; Breese, M. B. H.; Sherburne, M.; Asta, M.; Xu, Q.-H.; Venkatesan, T. Electron Transport and Visible Light Absorption in a Plasmonic Photocatalyst Based on Strontium Niobate. *Nat. Commun.* **2017**, *8*, 15070.
(15) Robatjazi, H.; Bahauddin, S. M.; Doiron, C.; Thomann, I. Direct Plasmon-Driven Photoelectrocatalysis. *Nano Lett.* **2015**, *15*, 6155−6161.
(16) Mubeen, S.; Lee, J.; Singh, N.; Krämer, S.; Stucky, G. D.; Moskovits, M. An Autonomous Photosynthetic Device in Which All Charge Carriers Derive from Surface Plasmons. *Nat. Nanotechnol.* **2013**, *8*, 247−251.
(17) Kumar, D.; Lee, A.; Lee, T.; Lim, M.; Lim, D. K. Ultrafast and Efficient Transport of Hot Plasmonic Electrons by Graphene for Pt Free, Highly Efficient Visible-Light Responsive Photocatalyst. *Nano Lett.* **2016**, *16*, 1760−1767.
(18) Ahmadi, T. S.; Logunov, S. L.; El-Sayed, M. A. Picosecond Dynamics of Colloidal Gold Nanoparticles. *J. Phys. Chem.* **1996**, *100*, 8053−8056.
(19) Brongersma, M. L.; Halas, N. J.; Nordlander, P. Plasmon-Induced Hot Carrier Science and Technology. *Nat Nanotechnol.* **2015**, *10*, 25−34.
(20) Zhang, Y.; He, S.; Guo, W.; Hu, Y.; Huang, J.; Mulcahy, J. R.; Wei, W. D. Surface-Plasmon-Driven Hot Electron Photochemistry. *Chem. Rev.* **2018**, *118*, 2927−2954.
(21) Valenti, M.; Venugopal, A.; Tordera, D.; Jonsson, M. P.; Biskos, G.; Schmidt-Ott, A.; Smith, W. A. Hot Carrier Generation and Extraction of Plasmonic Alloy Nanoparticles. *ACS Photonics* **2017**, *4*, 1146−1152.
(22) Ma, X. C.; Dai, Y.; Yu, L.; Huang, B. B. Energy Transfer in Plasmonic Photocatalytic Composites. *Light: Sci. Appl.* **2016**, *5*, No. e16017.
(23) Giugni, A.; Torre, B.; Toma, A.; Francardi, M.; Malerba, M.; Alabastri, A.; Proietti Zaccaria, R.; Stockman, M. I.; Di Fabrizio, E. Hot-Electron Nanoscopy Using Adiabatic Compression of Surface Plasmons. *Nat. Nanotechnol.* **2013**, *8*, 845−852.
(24) Yu, Y.; Ji, Z.; Zu, S.; Du, B.; Kang, Y.; Li, Z.; Zhou, Z.; Shi, K.; Fang, Z. Ultrafast Plasmonic Hot Electron Transfer in Au Nanoantenna/MoS_2 Heterostructures. *Adv. Funct. Mater.* **2016**, *26*, 6394−6401.
(25) Shan, H.; Yu, Y.; Wang, X.; Luo, Y.; Zu, S.; Du, B.; Han, T.; Li, B.; Li, Y.; Wu, J.; Lin, F.; Shi, K.; Tay, B. K.; Liu, Z.; Zhu, X.; Fang, Z. Direct Observation of Ultrafast Plasmonic Hot Electron Transfer in the Strong Coupling Regime. *Light: Sci. Appl.* **2019**, *8*, 9.
(26) Sousa-Castillo, A.; Comesaña-Hermo, M.; Rodríguez-González, B.; Pérez-Lorenzo, M.; Wang, Z.; Kong, X. T.; Govorov, A. O.; Correa-Duarte, M. A. Boosting Hot Electron-Driven Photocatalysis through Anisotropic Plasmonic Nanoparticles with Hot Spots in Au−TiO2Nanoarchitectures. *J. Phys. Chem. C* **2016**, *120*, 11690−11699.
(27) Wu, B.; Liu, D.; Mubeen, S.; Chuong, T. T.; Moskovits, M.; Stucky, G. D. Anisotropic Growth of TiO2onto Gold Nanorods for Plasmon-Enhanced Hydrogen Production from Water Reduction. *J. Am. Chem. Soc.* **2016**, *138*, 1114−1117.
(28) Zheng, Z.; Tachikawa, T.; Majima, T. Single-Particle Study of Pt-Modified Au Nanorods for Plasmon-Enhanced Hydrogen Generation in Visible to near-Infrared Region. *J. Am. Chem. Soc.* **2014**, *136*, 6870−6873.
(29) Ortiz, N.; Zoellner, B.; Hong, S. J.; Ji, Y.; Wang, T.; Liu, Y.; Maggard, P. A.; Wang, G. Harnessing Hot Electrons from Near IR Light for Hydrogen Production Using Pt-End-Capped-AuNRs. *ACS Appl. Mater. Interfaces* **2017**, *9*, 25962−25969.
(30) Xi, C.; Chen, Z.; Li, Q.; Jin, Z. Effects of H+, Cl- and CH3COOH on the Photocatalytic Conversion of PtCl62- in Aqueous TiO2 Dispersion. *J. Photochem. Photobiol., A* **1995**, *87*, 249−255.
(31) Liu, Y.; Gokcen, D.; Bertocci, U.; Moffat, T. P. Self-Terminating Growth of Platinum Films by Electrochemical Deposition. *Science* **2012**, *338*, 1327−1330.
(32) Kang, M.; Park, S. G.; Jeong, K. H. Repeated Solid-State Dewetting of Thin Gold Films for Nanogap-Rich Plasmonic Nanoislands. *Sci. Rep.* **2015**, *5*, 14790.
(33) Lee, Y. K.; Lee, H.; Lee, C.; Hwang, E.; Park, J. Y. Hot-Electron-Based Solar Energy Conversion with Metal-Semiconductor Nanodiodes. *J. Phys. Condens. Matter* **2016**, *28*, 254006.
(34) Macyk, W.; Burgeth, G.; Kisch, H. Photoelectrochemical Properties of Platinum(IV) Chloride Surface Modified TiO2. *Photochem. Photobiol. Sci.* **2003**, *2*, 322−328.
(35) Lord, H. L.; Zhan, W.; Pawliszyn, J. Fundamentals and Applications of Needle Trap Devices: A Critical Review. *Anal. Chim. Acta* **2010**, *677*, 3.
(36) Kong, X.-T.; Wang, Z.; Govorov, A. O. Plasmonic Nanostars with Hot Spots for Efficient Generation of Hot Electrons under Solar Illumination. *Adv. Opt. Mater.* **2017**, *5*, 1−10.
(37) Yu, Y.; Wen, W.; Qian, X. Y.; Liu, J. B.; Wu, J. M. UV and Visible Light Photocatalytic Activity of Au/TiO 2 Nanoforests with Anatase/Rutile Phase Junctions and Controlled Au Locations. *Sci. Rep.* **2017**, *7*, 41253.
(38) Zilio, P.; Dipalo, M.; Tantussi, F.; Messina, G. C.; De Angelis, F. Hot Electrons in Water: Injection and Ponderomotive Acceleration by Means of Plasmonic Nanoelectrodes. *Light: Sci. Appl.* **2017**, *6*, No. e17002.
(39) Lee, H.; Lee, H.; Park, J. Y. Direct Imaging of Surface Plasmon-Driven Hot Electron Flux on the Au Nanoprism/TiO 2. *Nano Lett.* **2019**, *19*, 891−896.
(40) Yu, W.; Porosoff, M. D.; Chen, J. G. Review of Pt-Based Bimetallic Catalysis: From Model Surfaces to Supported Catalysts. *Chem. Rev.* **2012**, *112*, 5780−5817.
(41) Shuang, S.; Lv, R.; Xie, Z.; Zhang, Z. Surface Plasmon Enhanced Photocatalysis of Au/Pt-Decorated TiO2 Nanopillar Arrays. *Sci. Rep.* **2016**, *6*, 26670.
(42) Radecka, M.; Wierzbicka, M.; Komornicki, S.; Rekas, M. Influence of Cr on Photoelectrochemical Properties of TiO2 Thin Films. *Phys. B* **2004**, *348*, 160−168.
(43) Kim, N. H.; Meinhart, C. D.; Moskovits, M. Plasmon-Mediated Reduction of Aqueous Platinum Ions: The Competing Roles of Field Enhancement and Hot Charge Carriers. *J. Phys. Chem. C* **2016**, *120*, 6750−6755.
(44) Santiago, D.; Rodríguez-Calero, G. G.; Palkar, A.; Barraza-Jimenez, D.; Galvan, D. H.; Casillas, G.; Mayoral, A.; Jose-Yacamán, M.; Echegoyen, L.; Cabrera, C. R. Platinum Electrodeposition on Unsupported Carbon Nano-Onions. *Langmuir* **2012**, *28*, 17202−17210.
(45) Scanlon, M. D.; Peljo, P.; Méndez, M. A.; Smirnov, E.; Girault, H. H. Charging and Discharging at the Nanoscale: Fermi Level Equilibration of Metallic Nanoparticles. *Chem. Sci.* **2015**, 2705−2720.

DOI: 10.1021/acsami.9b10913
ACS Appl. Mater. Interfaces 2019, 11, 35713−35719